# Chemical and physical aspects of the post-exposure baking process used for positive-tone chemically amplified resists

by W. D. Hinsberg F. A. Houle M. I. Sanchez G. M. Wallraff

Chemically amplified (CA) resists are in widespread use for the fabrication of leadingedge microelectronic devices, and it is anticipated that they will see use well into the future. The refinement and optimization of these materials to allow routine imaging at dimensions that will ultimately approach the molecular scale will depend on an improved in-depth understanding of the materials and their processing. We provide here an overview of recent work in our laboratory on the chemical and physical processes that occur during post-exposure baking (PEB) of positivetone CA resists. Our results provide a clearer understanding of how this critical step in the lithographic imaging process will affect extendibility of the CA resist concept to nanoscale feature sizes.

### Introduction

Advances in lithographic imaging techniques and materials have played a key role in the remarkable evolution of semiconductor devices and circuits, where the continuing drive toward miniaturization has led to improved performance and lower cost. Deep-ultraviolet (DUV) photolithography, first used in IBM in the 1980s, is now the standard imaging technique used for the production of the most advanced integrated circuits [1]. The development of chemically amplified (CA) resists [2] was key to the implementation of DUV lithography. The future evolution of DUV optical exposure tool technology, and the availability of advanced lithography systems based on electron, ion, or extreme ultraviolet exposure sources, will depend critically on further refinements in CA resists. In the future, lithography systems will be used with CA resists to print features at 50 nm and below, requiring an overall precision of 2-5 nm [3], an unprecedented level of control over image formation.

A schematic of the lithographic process using a positive-tone CA resist is shown in **Figure 1**. Because of diffraction, the radiation image that strikes the resist is significantly blurred compared to the original pattern defined by the mask. To print precise nanoscale features using this degraded image, the resist must respond in a nonlinear way to light intensity, and further image blurring

©Copyright 2001 by International Business Machines Corporation. Copying in printed form for private use is permitted without payment of royalty provided that (1) each reproduction is done without alteration and (2) the Journal reference and IBM copyright notice are included on the first page. The title and abstract, but no other portions, of this paper may be copied or distributed royalty free without further permission by computer-based and other information-service systems. Permission to republish any other portion of this paper must be obtained from the Editor.

0018-8646/01/\$5.00 © 2001 IBM

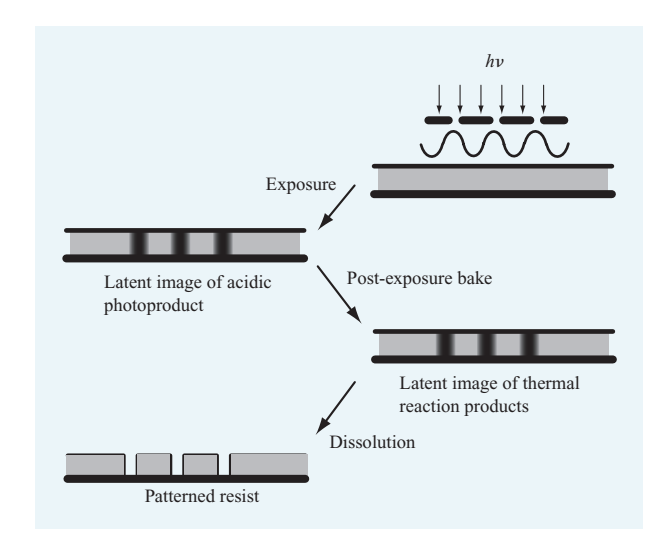


### Figure <sup>·</sup>

Schematic of the positive-tone CA resist lithographic process. A film of the polymeric resist is exposed to a patterned beam of radiation, creating an image of an acidic product in the film. A heating step activates the acid in a reaction that alters the solubility properties of the film in the irradiated areas. Washing the film with an appropriate developing solution produces a three-dimensional relief pattern that is then used in the formation of a single patterned layer of an integrated circuit.

and random fluctuations in linewidth introduced by the chemical and physical processes that occur during resist processing must be kept to a minimum. A growing number of reports have cited instances in which properties of the resist materials have limited the smallest feature size that can be achieved [4].

It is evident that considerable refinement of resists will be necessary to meet future performance demands. Today, our understanding of the chemical reactions that occur in the resist film following imaging exposure, while considerable, is not yet at a level of detail that will allow us to design the very high-performance photoresists required. We have made significant progress toward this end, however, and in this paper we provide an overview of our current work on understanding relevant, molecular-level chemical and physical aspects of CA resist processes. Our primary focus is on the origins of image blur for the specific case of positive-tone resists.

This paper is organized as follows. We first review the underlying operational principle of positive-tone CA resists in order to highlight the key chemical and physical elements that are to be considered in the design of resist systems. We then discuss the fundamentals of acid catalysis, chemical kinetics, and diffusion, with a specific focus on how resist reactivity is affected by the presence of the polymer medium. With this background, we briefly

describe previous studies of image blur in positive-tone CA resists, and then discuss in detail the results of our investigations of the way resist components work together to create an image.

### Imaging chemistry of positive-tone CA resists

Image formation in a positive-tone CA resist requires conversion of the polymer from an insoluble to a soluble form. Though the details of how this is achieved vary with resist design and the intended application, the imaging chemistry of all positive-tone CA resists is based on the sequence of transformations illustrated in Figure 2. The photosensitive iodonium salt depicted there acts as a photoacid generator, forming a proton-anion pair as one of its radiation products. That proton mediates a fragmentation or deprotection reaction of an ester, producing a carboxylic acid. The ester fragmentation also forms an unstable species, a carbocation, which ultimately deactivates by transferring the proton to another ester group on the polymer. In turn, this second ester group undergoes fragmentation as before, initiating a third cycle. This process of reaction and regeneration enables each proton to effect the deprotection of many ester groups in the polymer film [5], giving rise to an overall enhancement (or *chemical amplification*) of the initial latent image. In contact with an aqueous alkaline developer, the carboxylic acid groups formed during deprotection will ionize, rendering the polymer soluble in the aqueous solution.

### **Acid-catalyzed chemistry**

The proton formed in the reaction in Figure 2 is an acid. Virtually all positive-tone CA resist systems incorporate an acid catalyst in their imaging chemistry. A *catalyst* is a substance that participates in a particular chemical reaction and thereby increases its rate without itself undergoing any permanent change. Acid-catalyzed reactions can be described by a mechanism that includes the two generic reaction steps [6] in Scheme 1 below:

$$HA + S \rightleftharpoons HS^+ + A^-$$
 (Step 1)

and

$$HS^+ \to Products.$$
 (Step 2)

In Scheme 1, Step 1 represents a reversible reaction in which the reactant S and the acid catalyst HA combine to form a transient intermediate HS<sup>+</sup>. This unstable intermediate can undergo some chemical conversion to form a new product species (represented by Step 2), or Step 1 can reverse, regenerating HA and S. Depending on the relative rates of the two steps, chemists classify acid-catalyzed reactions as involving either *general acid catalysis* (when Step 2, the product-forming step, is fast compared to Step 1) or *specific acid catalysis* (when Step 2 is slow

$$\begin{bmatrix} (CH_3)_3C & & & \\$$

### Figure 2

Imaging chemistry of a typical positive-tone CA resist. In the first step, irradiation of the film triggers a photochemical reaction that produces an acidic product. The proton from this acid binds to an ester functional group attached to the polymer (shown in the second step). The protonation induces fragmentation of the labile ester group (the third step) in a manner that causes the ester to be replaced with a carboxylic acid and an unstable, transient carbocation to be formed. The carbocation releases a proton (the last step), which then protonates another ester group to repeat the last three steps of this sequence.

compared to Step 1). These terms have their roots in their differing kinetic behavior in buffer solutions when the concentration of the acid HA is changed [6].

Two types of acid-labile protecting groups have been widely used in positive-tone CA resist design: reactive esters, whose deprotection chemistry is shown in Figure 2, and ketals, whose acid-catalyzed hydrolysis is depicted in Figure 3. In solution, these reactions are considered to occur by specific acid catalysis [7]. Detailed kinetic analyses of positive-tone CA resist systems are also consistent with a specific acid catalysis mechanistic description in the resist film [8]. Therefore, the overall rate of deprotection is controlled by the rate of Step 2 in Scheme 1 and is proportional to the concentration of the protonated substrate intermediate HS<sup>+</sup> established by equilibration of that step. This concentration in turn depends on both the acidity of the acid HA (its ability to give up a proton), and the basicity of the substrate S (its ability to accept a proton). These properties can be quantified using the  $pK_a$  scale used to characterize acidity and basicity [9]. The  $pK_a$  value for the dissociation of an acid HA,

### Figure 3

General mechanism for acid-catalyzed hydrolysis of a ketal, a functional group widely used as the basis for imaging in positive-tone CA resists. Shown here is one possible sequence of steps (termed an A2 mechanism) leading to product formation; other sequences are possible. An initial rapid protonation of the ketal is followed by reaction of the protonated species with water to form a hemiketal and an alcohol. Under normal conditions, the hemiketal undergoes further reaction to produce a ketone as its final product.

$$HA \rightleftharpoons H^+ + A^-$$

is defined as the negative base-10 logarithm of the acid dissociation constant,

$$K_{\mathbf{a}} = \frac{[\mathbf{A}^{-}][\mathbf{H}^{+}]}{[\mathbf{H}\mathbf{A}]},$$

where the bracketed values [X] represent the equilibrium activity of the species X that we approximate here as its molar concentration. **Table 1** lists  $pK_a$  values for a selection of acidic functional groups found in CA resist compositions. The range of acid strengths of interest spans almost 20 orders of magnitude.

These  $pK_a$  values can be used to estimate the concentration of the protonated intermediate SH<sup>+</sup>. When Step 1 is in thermodynamic equilibrium, the relative concentrations of the species are given by the expression

$$K_{eq} = \frac{[A^{-}][SH^{+}]}{[HA][S]}.$$

**Table 1** Typical  $pK_a$  values for functional groups of importance in CA resist chemistry [9].

Functional group	Acidic form	Basic form	$pK_{\rm a}$
Triflic acid	CF <sub>3</sub> SO <sub>3</sub> H	CF <sub>3</sub> SO <sub>3</sub>	(>-12)
Aromatic ester	ArCOORH <sup>+</sup>	ArCOOR	-7.4
Aryl sulfonic	ArSO <sub>3</sub> H	ArSO <sub>3</sub>	-6.5
Aliphatic ester	RCOORH <sup>+</sup>	RCOOR	-6.5
Phenol	ArOH, <sup>+</sup>	ArOH	-6.4
Ether	$ArORH^{+}$	ArOR	-6
Carboxylic	$RCOOH_2^+$	RCOOH	-6
Ether	RORH <sup>+</sup>	ROR	-3.5
Amide	RCONR,H <sup>+</sup>	RCONR,	-0.75
Alkyl sulfonic	RSO <sub>3</sub> H	RSO <sub>3</sub>	0
Aryl amine	ArNHR,H+	ArNHR,	4
Carboxylic acid	RCOOH	RCOO -	5
Secondary amine	$R_2NH_2^+$	$R_2NH$	11

In terms of the acid-dissociation constants of the species involved, this can be written as

$$K_{\rm eq} = 10^{pK_{\rm a}^{\rm SH^+} - pK_{\rm a}^{\rm HA}},$$

using tabulated  $pK_a$  values for the acids HA and SH<sup>+</sup>. In a typical CA resist, the polymer comprises an acid-labile ester (SH<sup>+</sup> with  $pK_a \sim -7$ ) and a strong acid generated upon exposure (HA with a  $pK_a \sim -10$ ). Using typical concentrations of photogenerated acid HA (0.01 mol/liter) and substrate group S (6 mol/liter), the calculated concentration of undissociated acid HA is  $\sim 10^{-8}$  mol/liter. In this example, then, the proton resides exclusively on the acid-labile group in the form SH<sup>+</sup>, the initial concentration of which is determined by the amount of acid HA initially formed by exposure. In a positive-tone CA resist film of more complex composition, the protons distribute themselves among the components of the film matrix resin, acid labile groups, reaction products, and additives-in proportions determined by their individual concentrations and  $pK_a$  values. It is noteworthy that even weakly basic substances (amines and amides, for example) are completely protonated when in equilibrium with a strong acid and can disrupt the acid-catalyzed reaction. Because of this, extreme measures must be taken to protect CA resist films from inadvertent exposure to trace airborne quantities of such substances during processing [10].

### The rate constant

A catalyst serves to speed up the rate of a reaction but is not consumed by it. The increase in rate is accomplished by participation of the catalyst in the reaction to provide an alternate route to the products with lower-energy requirements. The rate R of a reaction is written as

$$R = k_{\text{obs}} \prod C_n,$$

where  $k_{obs}$  is the observed rate constant, and the  $C_n$ represent the concentrations of the reactants. The relationship between the rate of the reaction and its energy requirements is operationally defined in terms of the Arrhenius equation:  $k_{\text{obs}} = A \exp(-E_a/RT)$ , where A is termed the pre-exponential factor, R is the gas constant, T is absolute temperature, and  $E_{\perp}$  is the activation energy which expresses the temperature dependence of the rate constant [11]. Strictly speaking, the Arrhenius parameters A and  $E_a$ are fitting parameters for a set of data: They may or may not provide information on individual reaction events; the kineticist must determine whether or not the rate constant applies to a single elementary reaction step or a sequence of events. The values of  $E_a$  and A can readily be obtained experimentally by determining the rate constant at several temperatures and plotting  $\ln k_{\rm obs}$  vs. 1/T.

When applied to an elementary reaction step,  $E_{\rm a}$  can be thought of as corresponding roughly to the threshold energy for the reaction, and the pre-exponential factor A can be related to entropic requirements imposed as the reactants convert to products. In such cases, Arrhenius parameters for one reaction can be compared to values measured for other reactions with well-established mechanisms to provide information on the nature of the underlying chemical processes. **Table 2** lists typical activation parameters for several relevant types of reactions, illustrating their range of values [12, 13].

Rate constants for elementary reaction steps are portable quantities that are valid for more than one reaction system. Reaction models that are constructed from sequences of such elementary steps are powerful tools that can be extended to describe a wide range of reaction systems. On the other hand, phenomenological models, in which the rate constants are used simply as fitting parameters in a set of arbitrary equations unrelated to the underlying chemistry, can be used to evaluate only systems very close to those used for the initial fit. Because of this, physically based, chemically detailed models comprising elementary reaction steps are inherently more useful than phenomenological models.

# Kinetics of acid-catalyzed deprotection in solid polymer films

Most time-honored techniques for extracting elementary rate constants involve the use of dilute reagents and small overall extents of reaction. In the condensed phase, this typically means evaluating the initial rates and products of a reaction carried out in a large excess of liquid solvent. To understand how these conditions affect reactivity, imagine an acidic species and a compound that can undergo an acid-catalyzed reaction. Both are surrounded by a close-packed layer of solvent molecules, their solvation shell. The probability that two reagents will encounter each other during the course of their random

**Table 2** Arrhenius parameters for several chemical reactions [12, 13].

Reaction type	Example	A	$E_{\rm a}$ (kcal/mol)
Radical recombination	$2 \text{ CH}_3 \rightarrow \text{C}_2\text{H}_6$	$3 \times 10^{10} \; (M^{-1} \; s^{-1})$	0
Pyramidal inversion	NH <sub>2</sub>	<u> </u>	5.7
Alkene isomerization	$cis$ -stilbene $\rightarrow trans$ -stilbene	$2.5 \times 10^{10} \text{ (s}^{-1})$	36.7
Ester thermolysis	$CH_3CO_2$ -t-Bu $\rightarrow CH_3CO_2H + C_4H_8$	$2 \times 10^{13} \ (s^{-1})$	40.5
Nucleophilic substitution	$C_2^3H_5^2-Br+Cl^- \rightarrow C_2^2H_5^2-Cl+Br^-$	$8 \times 10^8  (\text{M}^{-1}  \text{s}^{-1})$	17.6

motions through the fluid is low, and to undergo reaction they must have the correct relative orientation so that internal motions of the complex lead to a transition state, then to products. The solvent shells must accommodate this close interaction so that a chemical reaction can occur. Once the complex has formed, its reaction followed by separation of the (solvated) products must be energetically favorable relative to simple separation of the complex back into the initial reactants. Products can be assumed to be inactive toward further reaction because their concentrations are very low.

In lithographic materials, however, reactions occur in the solid phase, with virtually no solvent present, and typically are carried out until large proportions of the reactants are consumed. Consider how the acid-catalyzed process will differ when the acid acts on the same functional group attached to a chain within a solid polymeric resist film. First, the concentrations of reactants and products typically are much higher than in solution, and secondary reactions considered to be negligible in dilute mixtures can occur to a significant extent. Specific relevant examples include the detection, via atmospheric pressure ionization mass spectrometry, of an unexpectedly complex mixture of volatile products formed during PEB of an exposed positive-tone CA resist [14] and the identification by NMR analysis of foreign polymer structures in CA resist films following PEB [15]. Second, compared to the solution state, molecular mobility is much reduced in a polymeric environment, and this can influence, for example, the encounter rates of reactants and the separation rates of nascent products, and can restrict the relative orientations of reactants that can be achieved in the encounter complex [16]. In consideration of these factors, there is no reason to expect that catalysis rates and product distributions occurring in a polymer film will be identical to those measured for the same reactants present in solution as small molecules and at low concentrations.

### **Diffusion**

Because the acid catalyst is produced in the resist film as a spatially nonuniform latent image, there are initial gradients in local concentrations of the photoproducts. As

**Table 3** Typical values for diffusion coefficients *D* [17, 18].

Diffusant	Medium	Temperature (°K)	$D (cm^2/s)$
Gas	Gas	273-298	0.1
Polar organics	Water	298	$1 \times 10^{-5}$
Не	Glass	298	$1 \times 10^{-10}$
Metal	Metal	298	$1 \times 10^{-16} - 1 \times 10^{-20}$
Air	Polymer	298	$1 \times 10^{-7} - 1 \times 10^{-9}$
Nonpolar organics	Polymer	310	$1 \times 10^{-7} - 1 \times 10^{-9}$
Polar organics	Polymer	315	$1 \times 10^{-9} - 1 \times 10^{-12}$
Ion pairs	Polymer	340	$1 \times 10^{-16} - 1 \times 10^{-18}$

the PEB process proceeds, the spatial distributions of acid catalyst, reactants, and products evolve in a complex manner, transforming the initial image. One of the processes influencing the final image is diffusion.

At a microscopic level, the diffusive process is a sequence of random movements of the diffuser relative to its surroundings. If the diffusant is spatially segregated, these random movements will tend to spread the diffusant out over the accessible volume until it is homogeneously distributed. Macroscopically, the kinetics are described by Fick's law,  $j = -D\nabla C$ , where j is the molar diffusion flux vector, D is the diffusion coefficient, and C is the molar concentration of the diffusing species. Thus, the diffusion rate is most strongly influenced by the degree of spatial segregation, or concentration gradient, and by the success rate of attempts at net displacement, as indicated by the magnitude of the diffusion coefficient.

Like all rate constants, a diffusion coefficient folds together a wealth of microscopic detail. Its magnitude is extremely sensitive to the phase of the medium (gas, liquid, or solid) for a given diffusant and to the chemical nature of the interaction between the diffusant and its surrounding atoms and molecules. Typical values are given in **Table 3**, illustrating the enormous range of values for different diffusant–medium systems [17, 18]. These influences are particularly complex in the case of movement through a reacting polymer film. As in all solids, an atom or molecule must have a vacant volume available in order to move from one location to another.

In general, such voids are created transiently in a polymer through fluctuations of the chains; as a result, the magnitude of the diffusion coefficient depends on the size of the diffusant and on the range of motion in the polymer. When the polymer is undergoing decomposition, as in a deprotection reaction, density changes can be large but are not instantaneous. The small molecules formed take time to diffuse out of the film or find energetically favorable traps, and may leave behind small voids that collapse only through polymer motion. These voids, or free volume, are known to play an important role in mediating transport through the polymer film [18]. The value of a diffusion coefficient can also be strongly dependent on experimental conditions. Environmental changes resulting from concentration-dependent interactions of the diffusant with the polymer or chemical reactions can affect the magnitude of the measured diffusion coefficients, leading to apparent concentration dependence, or non-Fickian behavior [18]. When this occurs, it signals clearly that diffusion is not all that is being measured.

How should we regard acid diffusion during the postexposure bake of a CA resist film? The acid in question is a proton, which never exists in isolation in the condensed phase. Its transport involves a series of transfers from trap to trap, either by direct transfer between pendant groups that come close to one another, or by transfer from a pendant group to a small molecule, which then moves to another pendant group and transfers the proton back to the polymer. The accessible proton transfer pathways are determined by the proton affinities of available small molecules and functional groups on the polymer, and the diffusion coefficient reflects any special requirements for relative orientation during transfer. Because there is no applied field and the acid is a positive ion, it cannot migrate far without the accompanying movement of a counter ion to maintain local electrical neutrality [18]. The counter ion in this case is formed during photolysis of the photoacid generator and has the same initial spatial distribution as the protons. Since the gradients are roughly the same, the rate of long-range diffusion depends primarily on the strength of the interaction between the ions and their local environment: transient density as well as chemical character. In the case of resists based on poly((t-butoxycarbonyloxy)styrene) (PTBOCST), for example, deprotection converts the polymer from a nonpolar to a polar environment, dynamically creating traps for polar and ionic small molecules and restricting their movement [19].

It is evident that the determination of a complete description of diffusion in CA resists is a formidable challenge. It is valid, however, to use a simplified model to study such systems if the properties and limitations of the measured coefficients are kept in mind.

# Literature on image spreading in positive-tone CA resists

Diffusion of the acid catalyst is often cited as a major factor in the image spreading, or blurring, that occurs during post-exposure thermal processing. Because this could potentially limit the extendibility of chemically amplified resists for fabrication of 50-nm-scale and smaller features, increasing attention has been given to the investigation of acid diffusion in resists. Acid diffusion is usually conceptualized as a process in which photogenerated ionic species undergo Fickian diffusion as a result of the very steep concentration gradients formed during imaging. As noted above, because diffusion is accompanied by reaction, the extraction of diffusion kinetics independent of deprotection kinetics is not simple. Numerous investigations of acid diffusion in positive-tone chemically amplified resist systems have been reported using the following to elucidate the coupled reaction-diffusion process: multilayer structures of acidified polymer or a layer of pure acid on pure polymer [20-22]; linewidth measurements [23, 24]; ionic conductivities [23, 25-27]; and spectroscopic probes of polymer chemistry changes during or after post-exposure bake [22, 23, 28–30]. Diffusion coefficients are typically obtained from the experimental measurements in one of three ways. The most detailed approach involves modeling the system using a coupled reaction-diffusion process, with diffusion represented by a Fickian process and a deprotection rate dependent on both the acid and remaining protected group concentrations [21, 22, 30–32]. Acid concentrations are not treated as constant, but undergo continuous reduction through loss processes. Simpler treatments involve the analysis of ionic conductivities [25-27] or material loss after development as a function of baking conditions [20, 24]. The diffusion coefficients reported in all of these studies are difficult to compare with one another directly because of the differences in polymer, photoacid generator (PAG) type and concentration, post-application bake (PAB) conditions, and PEB temperatures used; they range from  $10^{-15}$  to  $10^{-11}$  cm<sup>2</sup>/s. When these diffusion coefficients are converted into mean displacements, they indicate that the three-dimensional diffusion lengths that apply are of the order of 85 to 850 nm during a two-minute PEB at 80-100°C. These distances are large, suggesting that diffusion plays a significant role in determining feature width, and that printing 50-nm-wide patterns with CA resists should not be possible. How, then, can we explain the fact that such resists have been used to fabricate structures having minimum dimensions of 50 nm or less [4]? It is evident that acid diffusion and acid-catalyzed deprotection cannot be considered separately from one another, and simple interpretations of extent of reaction or ionic conductivity cannot be used to provide model-

independent reaction rate constants and diffusion coefficients that are physically based and can be used to guide thinking about resist formulations. A more useful approach is to determine an elementary description of the acid-catalyzed deprotection chemistry through a direct kinetics study of reactants and products formed in resist systems.

### Coupled reaction-diffusion kinetics of PEB

We have developed an approach to describing image spreading during PEB that contains the essential physical and chemical processes, and is extendible to new systems. Using in situ isothermal infrared (IR) spectroscopy, the PEB process is investigated in two stages, allowing the effects of chemical deprotection kinetics and acid diffusion to be analyzed separately [19, 33, 34]. First, the chemical kinetics of the deprotection processes are measured under conditions in which the acid is uniformly distributed in the polymer film (no gradient). This results in a quantitative description of the chemical kinetics of the system that is accurate over a wide range of temperatures, acid concentrations, and polymer compositions [8]. The kinetics measurement is then repeated on a second film in which the initial acid distribution is nonuniform. This is accomplished by irradiating a 1200-nm-thick, positivetone CA resist film with a 193-nm UV light source, a wavelength at which the film is very strongly absorbing, so that the penetration of light (and thereby the photogeneration of acid) is confined to a well-defined surface layer. The result is the formation of a thin ( $\sim$ 200nm-thick) layer of exposed resist containing acid at the surface of a much thicker (~1000-nm-thick) unexposed layer (Figure 4). If the photogenerated acid does not diffuse to a significant degree, only the initial acidified surface layer will undergo acid-catalyzed chemical changes, but if the acid does diffuse into the initially acid-free underlayer, both the surface layer and some portion of the underlayer will undergo the catalyzed chemical reaction. The overall extent of deprotection in the film can be readily quantified by monitoring the intensity of a characteristic absorption band in the IR spectral region. Since the chemical deprotection kinetics are precisely and quantitatively known, the details of acid transport can be extracted by comparing the experimental behavior of the system to that predicted by modeling using the diffusion coefficient as the only variable.

The CA resist chosen for study is based on PTBOCST, one of the simplest and best-characterized positive-tone CA resist polymers. Initially, PTBOCST was combined with di-(t-butylphenyl)iodonium perfluorobutanesulfonate (TBI-PFBS), a commonly used photoacid generator. TBI-PFBS generates perfluorobutanesulfonic acid (PFBS-A) upon irradiation. To model the IR results, the resist film was represented as a stack of 120 homogeneous

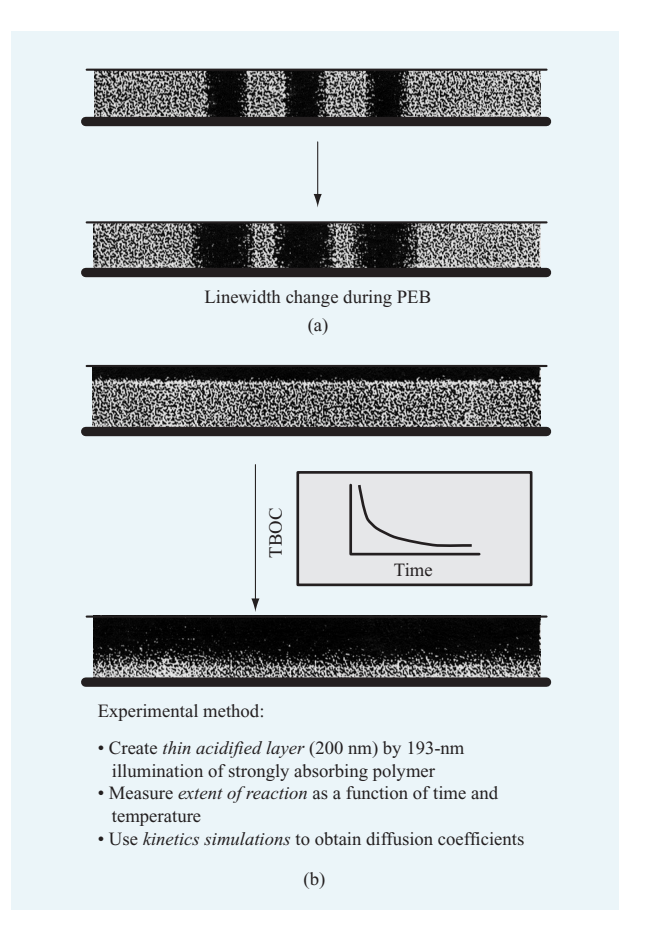


### Figure 4

Image blur in positive-tone CA resists: (a) Image spreading of an exposed feature during PEB. (b) Schematic of the experimental protocol used in this study to characterize the kinetics of image spreading.

polymer-PAG subfilms, each initially 10 nm thick and containing the fully protected polymer and a quantity of acid catalyst corresponding to that formed by the UV exposure (Figure 5). The effect of light attenuation by the strongly absorbing film is accounted for in the initial acid distribution. Within each subfilm the full set of thermal and acid-catalyzed deprotection reactions can take place, and transport of the acid can occur between adjacent subfilms. This model contains only the minimal elements judged necessary to describe the key chemical and physical processes that are occurring: those associated with the deprotection and the acid transport in the direction of its concentration gradient. Fick's law of diffusion is used to describe the concentration dependence of the transport rate. One anticipates that the mobility of the acid (an ionic species) in the nonpolar environment of the initial protected polymer will differ from that in the more polar environment produced when the polymer undergoes

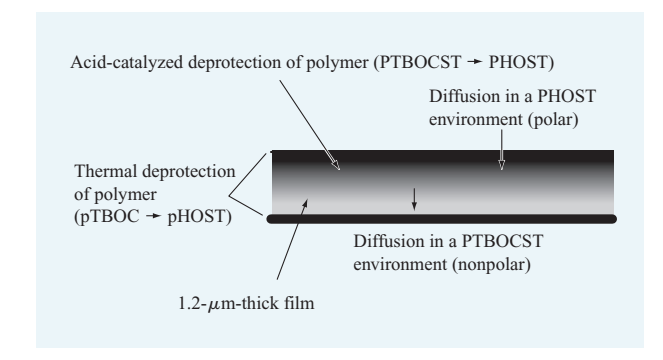


### Figure 5

Details of the model description used for reaction—diffusion simulation of the image-spreading experiments. The film is divided into 120 layers. The initial film thickness decreases continuously as deprotection proceeds because of the much higher density of PHOST. (Adapted from Reference [40], with permission.)

deprotection. This is modeled by using two diffusion coefficients to characterize transport in each of the two extremes, and assuming that at any point in time the overall diffusion rate is a combination of both pathways. Quantitative predictions of the time evolution of this model system were carried out using an in-house kinetics simulator program, specifically customized to correctly describe acid transport in an immobile polymer environment [19, 34].

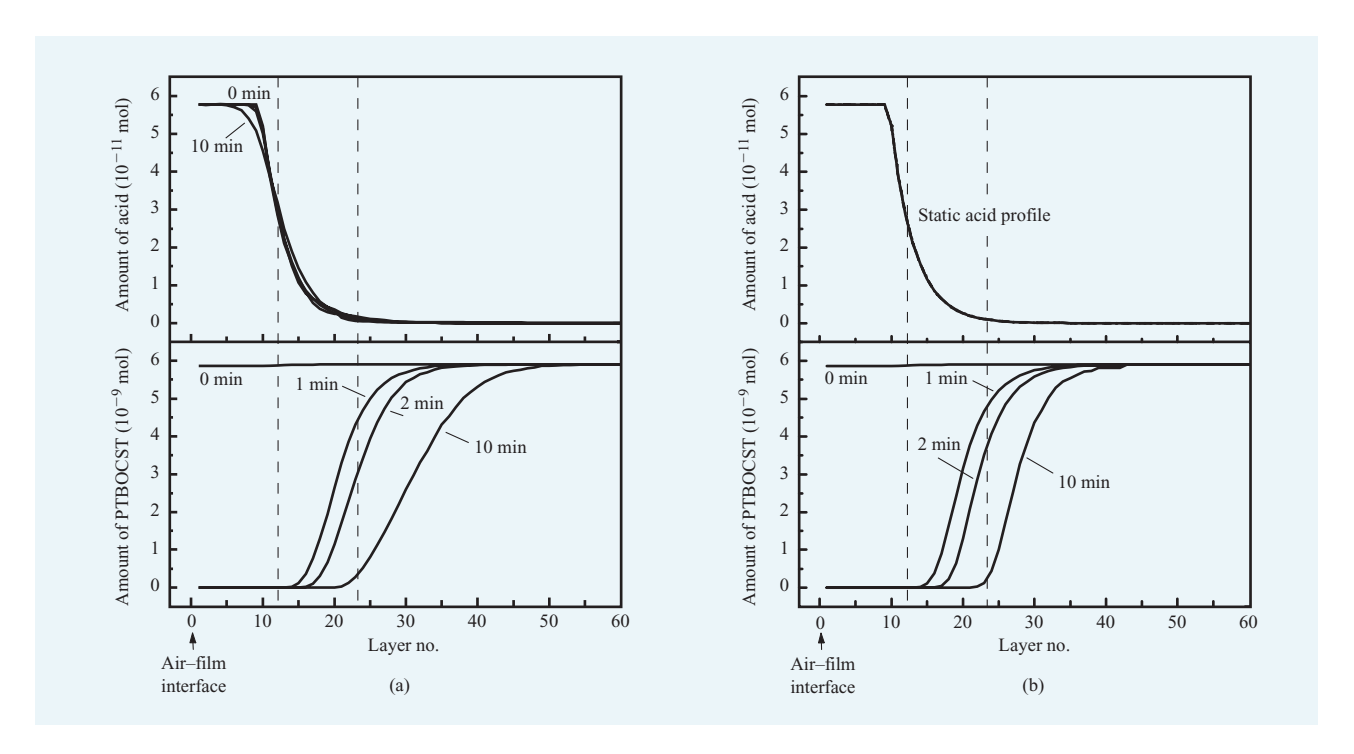
Using this simple model, we have derived a self-consistent description that accurately replicates our kinetics measurements. In that description, the diffusion coefficient of PFBS-A in the initial protected PTBOCST polymer increases from a value of  $D_{\text{TBOCST}} = 0.15$  to 15 nm<sup>2</sup>/s as the temperature increases from 65°C to 105°C; the temperature dependence yields an activation energy for  $D_{\mathrm{TBOCST}}$  of 36.5 kcal/mol. The mobility of PFBS-A decreases sharply as the polymer undergoes deprotection. In the fully deprotected polymer [largely poly(hydroxystyrene), or PHOST], the diffusion coefficient  $D_{\text{HOST}} = 0.004 - 0.1 \text{ nm}^2/\text{s}$ over the 65-105°C temperature range, consistent with an activation energy for  $D_{\rm HOST}$  of 22.1 kcal/mol. The diffusion coefficients are much smaller than might have been expected. During a typical PEB process step (100°C for 120 s), the effective acid diffusion length is of the order of 5 nm.

Figure 6 shows calculated composition profiles, derived from reaction—diffusion analysis, that depict how the film composition evolves during the experiment. Figure 6(a) (top) shows how the initial acid distribution in the film changes at different points during a 600-s PEB at 100°C. Figure 6(a) (bottom) shows the concurrent evolution of the deprotection reaction, measured by the number of TBOC protecting groups remaining on the polymer. While

the acid profile shows only very slight relaxation during PEB, the "front" of the deprotection reaction moves substantially with time; in this particular circumstance, the front has moved  $\sim 100$  nm in two minutes. Figure 6(b) presents the behavior predicted for the hypothetical case in which the acid catalyst is stationary (that is, its diffusion coefficients  $D_{\mbox{\tiny TBOCST}}$  and  $D_{\mbox{\tiny HOST}}$  are equal to zero). Even under such limiting conditions, the calculations indicate that the deprotection front advances substantially into the film as the PEB step proceeds. In fact, these profiles are virtually indistinguishable from those of Figure 6(a) until more than two minutes have elapsed. Since the profile of deprotected polymer defines those regions of the film that are removed during resist development, its behavior is of primary practical interest. Our analysis indicates that there is significant spreading of the profile of deprotected polymer with increasing PEB time, far in excess of that expected on the basis of acid diffusion alone. In the case of a line printed in a resist film, this spreading would be manifested as an apparent increase in linewidth, or image blur, with increasing PEB time.

This spreading has its origins in the kinetics of the acid-catalyzed deprotection reaction. The rate of the deprotection reaction is an increasing function of the concentration of acid. In the highly exposed region near the film-air interface, the acid concentration is at its maximum, and so is the deprotection rate. At a depth of about 150 nm, the calculated acid concentration begins to decrease with increasing depth because of the attenuation of the exposing radiation. This in turn causes a gradient in the rate of the deprotection reaction in this region, with some diffusion occurring and the local rate of deprotection slowing with increasing depth as the local acid concentration drops. The calculated polymer composition in this region changes more slowly than near the film-air interface, contributing to image spreading at longer times. While Figure 6 demonstrates that the diffusion of acid can increase the rate with which the spreading occurs, in this instance it constitutes a minor contribution to overall spreading of the deprotected polymer layer on the time scale typical of PEB processing. Thus, image spreading during PEB in this case is caused by the very high efficiency of the catalytic processes.

What is the significance of this result for lithographic imaging? The initial acid profile created in the surface-exposure experiment, a region of high acid concentration that gradually tapers to an area of low concentration, is exactly like that formed upon imaging a positive-tone CA resist using projection lithography, a consequence of diffraction at the edge of a mask feature. To understand the influence of chemical processes on imaging, we have performed reaction—diffusion simulations for a series of line—space arrays, exposed with a sinusoidal aerial image similar to those found



Fiaure 6

Calculated profiles for total acid (upper graphs) and PTBOCST (lower graphs) for PEB at 100°C in the surface-exposure experiment. Molar amounts in each layer are plotted, scaled as indicated. (a) Calculations with both reaction and diffusion enabled. (b) Calculations with only reaction enabled.

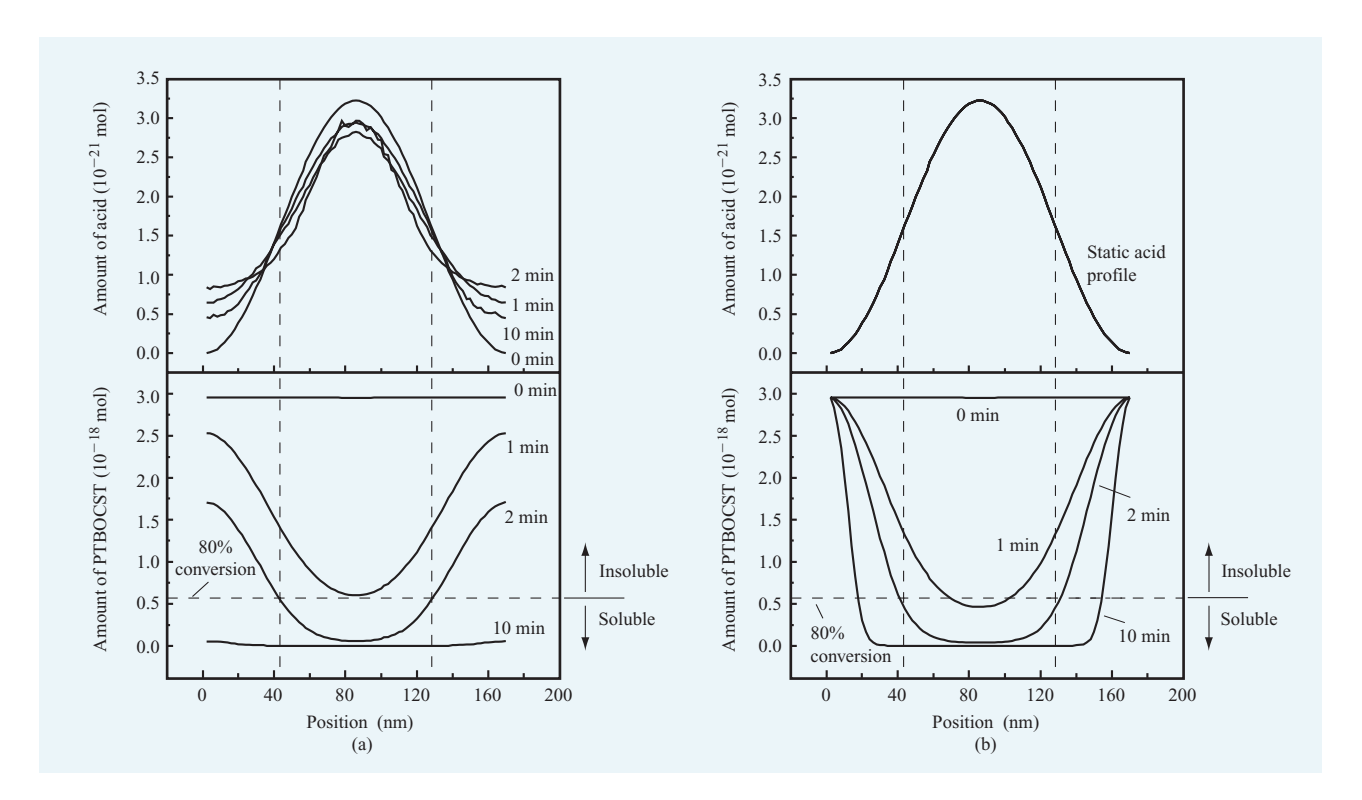
in projection lithography. The selected exposure and PEB process conditions were typical of those used with PTBOCST resist. Figure 7 illustrates simulation results for a specific case in which the array was set to 85-nm lines/85-nm spaces. The upper curves of Figure 7 depict the evolution of the acid profile during PEB, and the lower curves show the evolution of the profile of deprotected polymer. The polymer is considered to be soluble in developer when the amount of PTBOCST has dropped below 20 mole percent, that is, when the deprotection reaction is at least 80 percent complete. The limit at which solubility is achieved is indicated by horizontal dashed lines; the regions in which a curve falls below that line are soluble and are removed upon resist development. Thus, the sets of curves can be used to describe how linewidth decreases and space width increases with increasing PEB time.

Figure 7(a) presents simulation results for the case in which the acid-diffusion kinetics are those derived from our experimental measurements. Figure 7(b) shows the same profiles for the case in which the acid catalyst is stationary; that is, the diffusion coefficients are set equal to zero. Though Figure 7(a) shows that the initial acid profile does undergo some relaxation during PEB due to diffusion, a comparison of the time evolution of the

deprotected polymer profiles to the hypothetical nondiffusing case of Figure 7(b) leads to the conclusion that, at these feature dimensions, the practical impact of acid diffusion on linewidth is negligible under typical resist-processing conditions.

What happens as linewidths decrease? Figure 8 summarizes predictions of the way in which image spreading changes as a function of image size. This was assessed by repeating the PEB image simulations depicted in Figure 7 for a range of different feature sizes. By executing two sets of simulations at each geometry, one using acid-diffusion coefficients derived from our experimental study, and a second in which acid was considered to be stationary, the individual contributions of the chemical deprotection kinetics and of acid diffusion to overall image spreading could be estimated. These quantities are plotted in Figure 8 as a fraction of the nominal image linewidth.

The data of Figure 8 indicate that the contribution of the deprotection chemical processes to image spreading is a *constant fraction* of the image size. Recall that the chemical component of image spreading is due to the small but nonetheless kinetically significant quantities of acid catalyst created by diffraction outside the boundaries of the nominal printed line. The initial acid spatial



## Figure 7

Simulated spatial profiles for total acid (upper curves) and PTBOCST (lower curves) for PEB at 100°C in a projection-exposed 170-nm-pitch line–space array. The film was divided into 85 vertical layers for this simulation. Molar amounts for each layer are plotted, scaled as indicated. (a) Calculations with both reaction and diffusion enabled. (b) Calculations with only reaction enabled. (Adapted from Reference [40], with permission.)

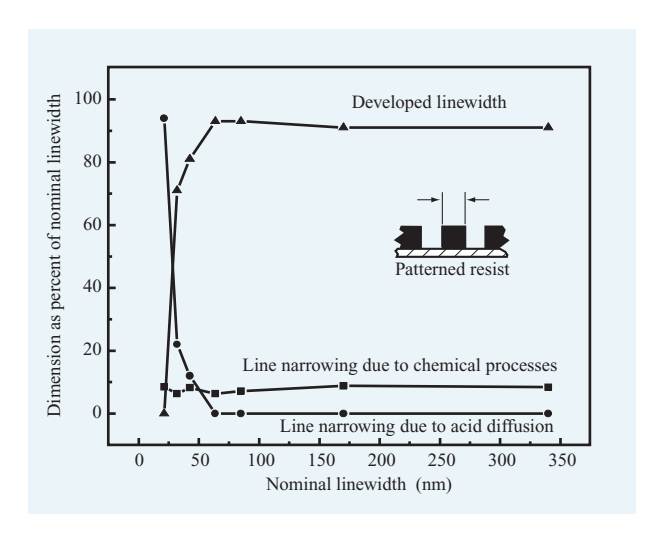


### Figure 8

Contributions of deprotection chemical processes and acid diffusion to image spreading in PTBOCST/TBI-PFBS resist. (Adapted from Reference [40], with permission.)

distribution formed with a sinusoidal aerial image scales with that image, so the relative extent of reaction for a given exposure dose is constant. If the spatial dimensions of the aerial image are scaled, then so is the initial spatial distribution of acid in the film, and with it, the effects of that distribution. For the particular material and process conditions chosen here, the chemical component of image spreading produces a constant image bias of about seven percent.

At linewidths greater than 70 nm, the data of Figure 8 indicate that the contribution of acid diffusion to image spreading is negligible. The diffusion processes have an intrinsic distance scale, however, of the order of 5 nm under the conditions used here; hence, acid diffusion should become important when the image dimension approaches that scale. This is borne out in Figure 8. At feature dimensions near 40–50 nm, the contribution of acid diffusion to image spreading is equivalent to that of the evolution of deprotection processes, and that contribution increases sharply as feature size decreases further. For the specific resist composition and process

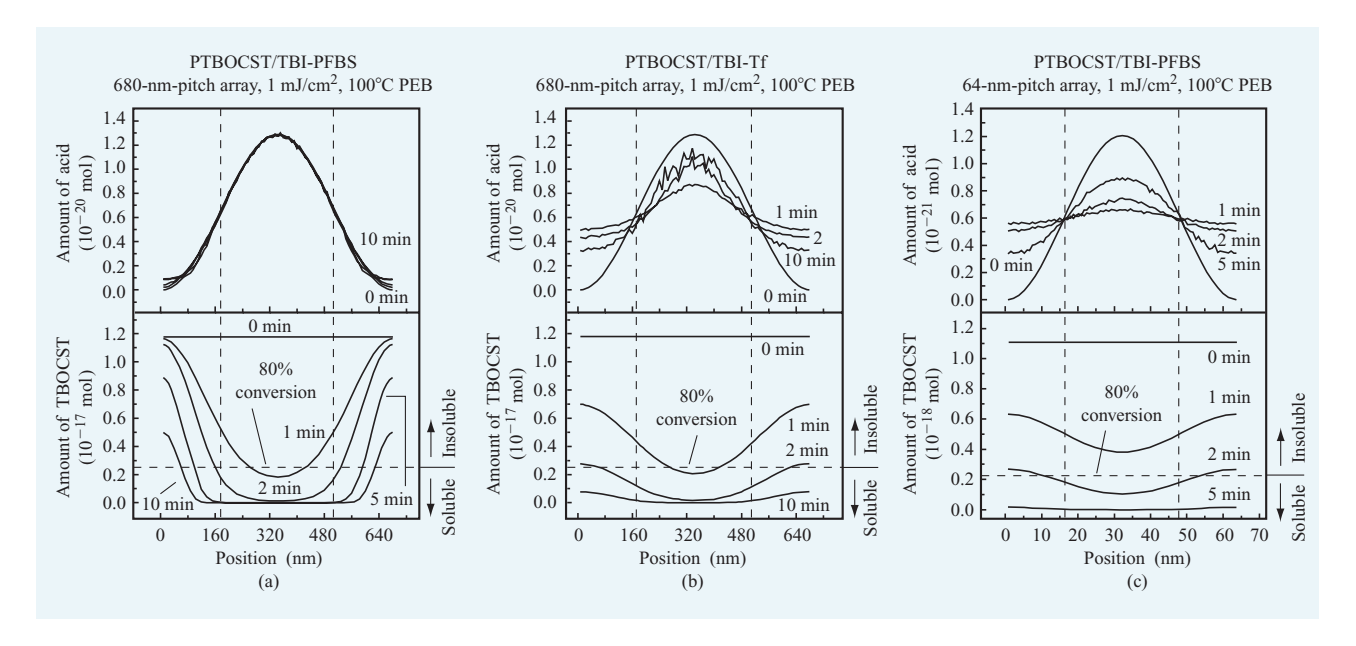


Figure 9

Comparison of predicted spatial profiles for PTBOCST resist containing TBI-PFBS and TBI-Tf. (Adapted from Reference [40], with permission.)

conditions treated in this exercise, we estimate that, given a sufficiently high-contrast resist-development process, the limits of spatial resolution would be in the range of 30 nm. We have created similar plots for other combinations of resist components, and they have all shown similar behavior. Although quantitative details vary with formulation, exposure, and bake conditions, the trends are similar: At large linewidths, line narrowing is governed by chemical processes, and at small linewidths, it is governed by diffusion.

### Impact of anion size on image spreading

Factors that control diffusant mobility include its shape, structure, and size [35]. We have characterized the kinetics of deprotection and acid diffusion in a second PTBOCST resist composition in which the TBI-PFBS photoacid generator was replaced with its close homolog di-(t-butylphenyl)iodonium trifluoromethanesulfonate (TBI-Tf). TBI-Tf was chosen for study because its key chemical properties are essentially identical to those of TBI-PFBS: Their efficiencies for photoacid generation are the same, and the trifluoromethanesulfonic acid (Tf-A) produced upon irradiation of TBI-Tf is a strong acid equivalent in acidity to PFBS-A. The size of Tf-A, however, as measured by its calculated molecular volume [33], is smaller than that of PFBS-A by more than a factor of 2. This provides a means of assessing the impact of molecular size on the diffusion component of image blur. We find that while the kinetics of the acid-catalyzed deprotection reaction differ only slightly from those determined for the PTBOCST/TBI-PFBS resist, the

diffusion characteristics of the two acids show pronounced differences. The diffusion coefficients for the smaller Tf-A are larger by factors of 9 to 70, depending on temperature, than the corresponding values for PFBS-A. The measured activation energies for diffusion of the two species are the same within the uncertainty of our analysis, suggestive of a common mechanism for diffusion in the two systems.

Of practical interest is how the increased mobility of Tf-A is manifested in lithographic imaging properties. Figure 9(a) shows predicted spatial profiles for one period of a dense line-space array of 680-nm pitch, as printed in PTBOCST/TBI-PFBS resist, using the conditions of Figure 7. Changes in the distribution of acid in the film, and in the extent of acid-catalyzed deprotection as measured by the amount of TBOCST remaining, are shown. At this dimensional scale, the PFBS-A acid is effectively stationary, and the profile of deprotected polymer evolves and spreads under control of the kinetics of acid-catalyzed deprotection. Figure 9(b) shows the same spatial profiles printed in PTBOCST/TBI-Tf resist. In this case, the profile of acid (Tf-A) undergoes a rapid and pronounced change, a consequence of its higher mobility. This has a large impact on the developable profile of deprotected polymer, as shown in the lower portion of Figure 9(b). For comparison, Figure 9(c) shows predicted spatial profiles for PTBOCST/PFBS-A resist for a line/space array of 64-nm pitch; the profiles are roughly equivalent in appearance to those for PTBOCST/TBI-Tf patterned at a pitch of 680 nm. The simulations indicate that the

increased mobility of Tf-A degrades achievable resolution by roughly an order of magnitude compared to PFBS-A.

We have examined other PAG systems in which the "spectator" anion is larger than the PFBS ion. In such cases, the mobility of the acid is reduced below the already low values found for PFBS-A, an indication that further attenuation of the limiting role of acid diffusion should be achievable. Consideration of the limiting case in which diffusion is negligible highlights the role deprotection kinetics play in image spreading. This is a consequence of the catalytic nature of the imaging process, which allows even very small amounts of acid to produce substantial deprotection. In the future, as we approach the dimensional limits of CA resists, there is the possibility that a tradeoff between sensitivity and resolution will be required, even in the absence of significant diffusion. The model described here provides a framework to examine that tradeoff.

### Role of added base during PEB

Adding small quantities of bases to positive-tone CA resist formulations has been reported to lead to longer shelf life and increased image resistance to airborne chemical contamination and substrate contamination effects, as well as imparting improved lithographic imaging properties [36–39]. The role of the bases has generally been described as acting as a trap for acid that diffuses from the exposed into the unexposed area. We have seen, however, that for a typical photoacid (e.g., PFBS-A in the PTBOCST system), acid diffusion is not the primary cause of image spreading. How, then, does an added base affect imaging?

We have addressed this question experimentally by adding to the PTBOCST/TBI-PFBS resist formulation varying small amounts of tetra-*n*-butyl ammonium hydroxide (TBA-OH)<sup>1</sup> [40]. The reaction and diffusion kinetics of the resulting mixtures were then characterized using the protocol described above. As expected, the addition of a base leads to a reduction in the amount of acid catalyst and thereby reduces the extent of deprotection. A more detailed and quantitative analysis of the effect of base can provide insight into the nature of underlying chemical processes. To facilitate this, our numerical description of TBI-PFBS/PTBOCST PEB was extended to include an acid-base neutralization step in each sublayer:

 $A + B \rightarrow$  inert neutralization product,

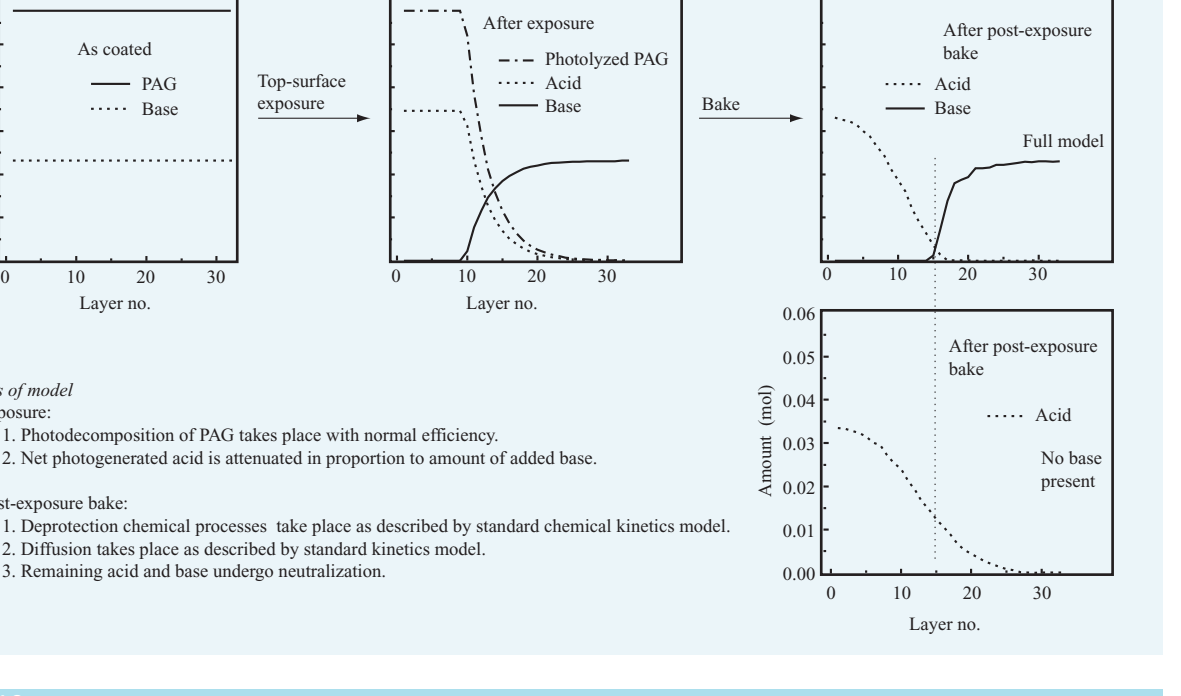
with kinetics described by the second-order rate law  $R_n = k_n[A][B]$ , where  $k_n$  is the rate constant for neutralization at a given temperature, and [A] and [B] are the instantaneous local concentrations of acid and base, respectively, at a specified location in the resist film.

We have simulated a variety of different models for the interaction of base with PAG and photogenerated acid, each differing in the assumptions made about the initial state of the film and rates for acid-base neutralization. The time evolution of the film was found to be a sensitive function of these assumptions, with each model predicting a distinctly different form of response to added base. Of those cases examined, only one description, which we term the proportional neutralization (PN) model, correctly reproduces experimental data. In the PN model (Figure 10), added base causes an initial proportional reduction in the amount of acid available immediately after photolysis and prior to PEB, the net effect being uniform attenuation of the acid profile. The acid and base distributions that remain are able to undergo further neutralization during PEB. It is assumed that the base does not diffuse appreciably.

The only parameter in the PN model not available from independent experimental analysis is  $k_n$ , the rate constant for acid-base neutralization. Its value must be constant at a given temperature and invariant with the amount of added base. Given these constraints, best-fit estimates of  $k_n$  were extracted by comparing predictions of the PN model to experiment. We have found that the PN model provides an accurate quantitative description of the effect of base on deprotection, with the extracted values of  $k_n$ being consistent with those expected for a diffusioncontrolled neutralization reaction of PFBS-A acid with a stationary base [41]. As an additional test, PTBOCST/TBI-PFBS films were exposed using 254-nm UV light, a wavelength at which the resist is much more weakly absorbing, in order to create a uniform acid distribution. The deprotection kinetics are correctly predicted using the PN model.

It is instructive to apply the PN model to understand how the addition of a base influences the evolution of deprotection. Figures 11(a) and 11(b) address the surface-exposure experiment. Part (a) shows the predicted evolution of deprotection for the standard case in which no base was added to the resist film. At the highly exposed region of the film, close to the air–film interface, the acid concentration is high, causing deprotection to proceed rapidly, quickly reaching 100% deprotection. Moving into the bulk of the film, the acid concentration drops, and the rate of deprotection slows, but remains high enough that the difference in polymer composition (its

<sup>&</sup>lt;sup>1</sup> Although the ionic base initially added to the resist solution is pure TBA-OH, there is evidence from work at IBM (unpublished) and from U.S. Patent 5,879,856 that it undergoes rapid reaction and is unlikely to be the sole base in the films prepared from the resist. The specific chemical identity of the base is unimportant for our model; it matters only that basic species be present in the resist solution. The number of equivalents of base present on the addition of a given amount of TBA-OH is determined explicitly for each resist formulation. It should be noted that TBA-OH is an ionic base, and some of the details of its behavior may differ from those of a nonionic base such as an amine. This possibility is currently under investigation in our laboratory.



0.06

0.05

0.04

0.03

0.02 0.01 0.00

Elements of model

Exposure:

Post-exposure bake:

Amount (mol)

As coated

10

- PAG

20

Layer no.

30

1. Photodecomposition of PAG takes place with normal efficiency.

2. Diffusion takes place as described by standard kinetics model.

3. Remaining acid and base undergo neutralization.

2. Net photogenerated acid is attenuated in proportion to amount of added base.

···· Base

Top-surface

exposure

Schematic description detailing key elements of the PN model used in this work. After coating, the PAG and base are present at a concentration that is uniform with depth in the resist film. During exposure, the PAG undergoes photolysis with normal efficiency, but in this instance the presence of the base causes an overall reduction in the amount of acid formed, yielding an initial acid profile whose magnitude is reduced in proportion to the amount of based added. The initial base profile at time = 0 is determined by accounting for the base consumed by this proportional neutralization. (Adapted from Reference [40], with permission.)

After exposure

···· Acid

20

Layer no.

30

Base

chemical contrast) between the lightly exposed regions and the strongly exposed regions continues to degrade with time.

Figure 11(b) shows the case in which TBA-OH base (0.4 molar equivalents relative to the peak amount of photoacid) was included in the formulation. As in part (a), the highly exposed levels of the film undergo rapid deprotection. In the lightly exposed levels, however, acid-base neutralization is sufficiently rapid that a reduction in overall rate of deprotection results. The functional impact of this approach is increased chemical contrast between strongly and lightly exposed regions, which does not degrade significantly with time.

Figures 11(c) and 11(d) show predicted behavior during imaging of a line/space array having a pitch of 170 nm. Part (c) presents the time evolution of deprotection for the case of base-free PTBOCST/TBI-PFBS resist. Also shown is the initial acid distribution formed upon exposure. Polymer deprotection occurs rapidly in the center of the exposed line, and also occurs, albeit at a slower rate, in the nominally unexposed areas. After 120 seconds at 100°C, the center of the exposed line is completely deprotected, and the center of the unexposed

area is deprotected to an extent of  $\sim$ 43%. Figure 11(d) depicts the case in which TBA-OH base was included in the PTBOCST/TBI-PFBS resist formulation (again at a level of 0.4 molar equivalents relative to the peak amount of photoacid). In this case the exposure dose was increased so that the initial acid-concentration profiles were identical to that of Figure 11(c). This acid distribution and the distribution of base predicted by the PN model at the start of PEB are overlaid on this plot. While deprotection in the center of the exposed line shows an evolution essentially identical to that in Figure 11(c), deprotection in the unexposed region is strongly suppressed; only ~13\% deprotection has taken place after 120 seconds. The increased chemical contrast between exposed and unexposed areas translates into improved discrimination between exposed and unexposed regions during development.

### **Summary and outlook**

In this paper, we have sought to give the reader an intuitive feeling for the way in which CA resist

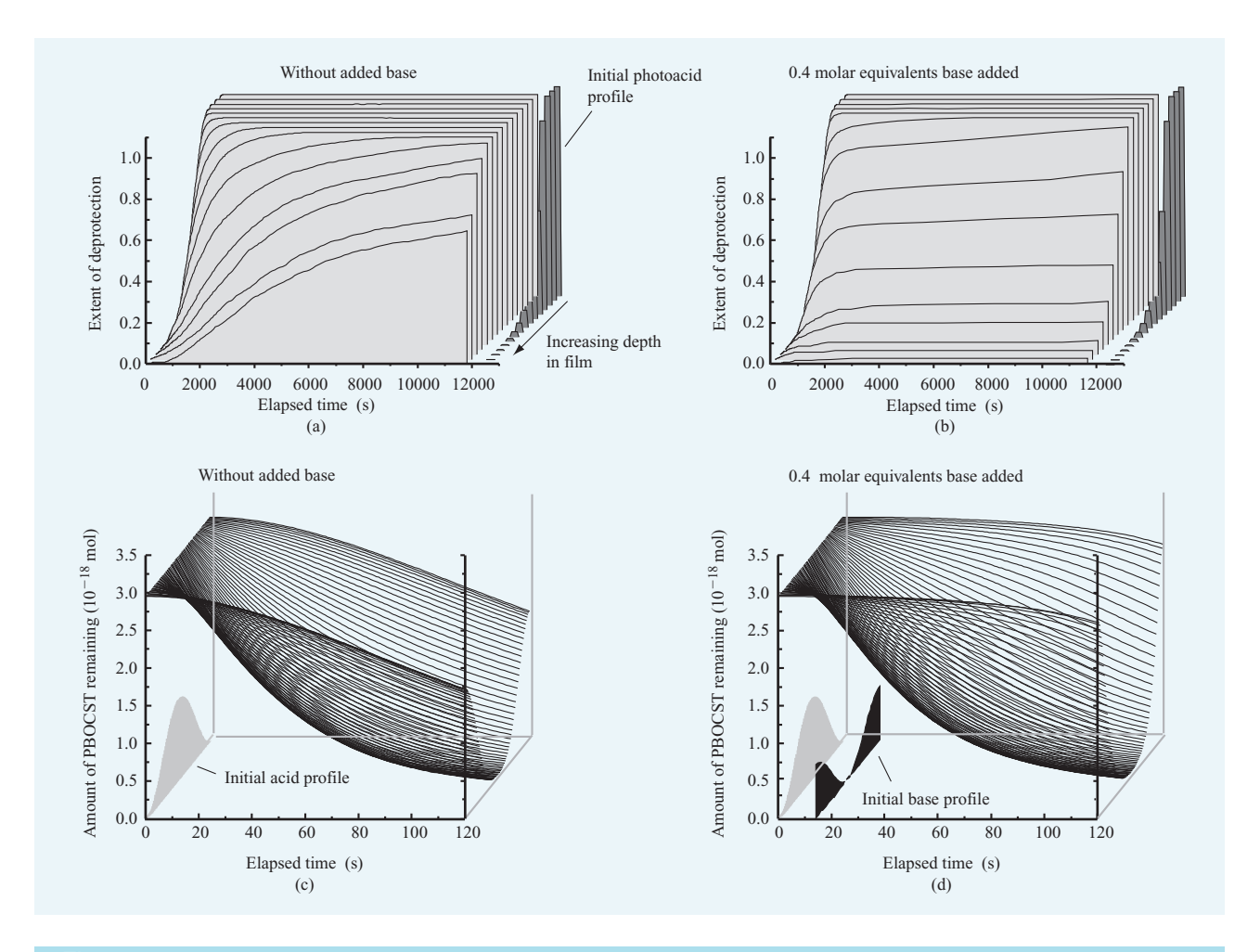


Figure 11

Predicted impact of added base and of diffusion on lithographic imaging of PTBOCST/TBI-PFBS resist using the PN model. Parts (a) and (b) show the extent of deprotection as a function of time, at different film depths for the surface exposure experiment. Parts (c) and (d) show the extent of deprotection, without and with added base, for lithographic imaging of a line/space array having a pitch of 170 nm.

components—polymer, acid, and base—interact to create a developable image, with a particular emphasis on the roles of acid—base chemistry and reaction kinetics during PEB. In experimental studies of the post-exposure bake process in a model resist formulation, we have applied these concepts to gain a better understanding of the chemical factors controlling image formation. This illustrates the value of a combined experimental—simulation approach to the characterization of the chemical behavior of a CA resist. Systematic development of an extendible, chemically accurate model, even for a simple model resist system, has allowed us to gain new insights into the connection between chemical changes and image formation in CA resists, and has improved our understanding of observations reported in the literature.

In the work described here, the key materials characteristics under study could be understood by treatment of the resist film as a continuous, homogeneous mixture with bulk-like physical properties. As minimum feature sizes shrink, and film thicknesses scale proportionately, we anticipate that interfacial effects will influence all stages of the lithographic process. Moreover, convergence of the critical dimension scale with the molecular scale will bring into play molecular size effects, both from the polymer molecules themselves and from local inhomogeneities. We believe that the refinement of resist materials for nanoscale imaging will demand a still greater depth of understanding, at the molecular scale, of their structure, properties, and dynamic behavior.

### **Acknowledgments**

We are grateful to our colleagues, John Hoffnagle, Michael Morrison, Michelle Poliskie, Hiroshi Ito, Sarunya Bangsaruntip, Phillip Brock, Gregory Breyta, and Dean Pearson, for numerous discussions and contributions to this research. This work has been supported in part by National Science Foundation Grant DMR-9400254 (CPIMA), which provided fellowships for Michael Morrison and Michelle Poliskie.

### References

- S. J. Holmes, P. H. Mitchell, and M. C. Hakey, *IBM J. Res. & Dev.* 41, 7 (1997).
- 2. H. Ito, IBM J. Res. & Dev. 41, 69 (1997).
- 3. International Technology Roadmap for Semiconductors, 1999 Edition, Semiconductor Industry Association; see http://member.itrs.net/Files/1999\_SIA\_Roadmap/Home.htm.
- G. M. Wallraff and W. D. Hinsberg, Chem. Rev. 99, 1801 (1999).
- D. R. McKean, U. Schaedeli, and S. A. McDonald, J. Polymer Sci. A 27, 3927 (1989).
- T. H. Lowry and K. S. Richardson, Mechanism and Theory in Organic Chemistry, Third Edition, 1987, Harper & Row, New York, Ch. 7.
- H. Maskill, *The Physical Basis of Organic Chemistry*, Oxford University Press, Oxford, England, 1989, p. 322.
- 8. G. Wallraff, J. Hutchinson, W. Hinsberg, F. Houle, P. Seidel, R. Johnson, and W. Oldham, *J. Vac. Sci. Technol. B* 12, 3857 (1994).
- 9. J. March, Advanced Organic Chemistry: Reactions, Mechanism and Structure, Third Edition, John Wiley & Sons, New York, 1985, Ch. 8.
- 10. S. MacDonald, W. Hinsberg, R. Wendt, N. Clecak, and G. Willson, *Chem. Mater.* **5**, 348 (1993).
- 11. K. Laidler, *Chemical Kinetics*, Third Edition, Benjamin Cummings, New York, 1989.
- 12. S. W. Benson, *Thermochemical Kinetics*, Second Edition, John Wiley & Sons, New York, 1976.
- A. Rank, L. C. Allen, and K. Mislow, *Angew. Chem. Int. Ed. Engl.* 9, 4004 (1970).
- F. A. Houle, G. M. Poliskie, W. D. Hinsberg, D. Pearson, M. Sanchez, H. Ito, and J. Hoffnagle, SPIE Advances in Resist Technology and Processing XVII 3999, 181 (2000).
- H. Ito and M. Sherwood, SPIE Advances in Resist Technology and Processing XVI 3678, 104 (1999).
- G. M. J. Schmidt, Pure Appl. Chem. 27, 647 (1971); J. M. Thomas, ibid., 51, 65 (1979); L. R. MacGillivray and J. L. Atwood, Angew. Chem. Int. Ed. 38, 1018 (1999); New Directions in Solid State Chemistry, C. N. R. Rao and J. Gopalakrishnan, Cambridge University Press, Cambridge, England, 1986.
- 17. R. B. Bird, W. E. Stewart, and E. N. Lightfoot, *Transport Phenomena*, John Wiley & Sons, New York, 1960.
- 18. J. Crank and G. S. Park, Eds., *Diffusion in Polymers*, Academic Press, London, 1968.
- F. A. Houle, W. D. Hinsberg, M. Morrison, M. I. Sanchez, G. Wallraff, C. Larson, and J. Hoffnagle, *J. Vac. Sci. Technol. B* 18, 1874 (2000).
- L. Schlegel, T. Ueno, N. Hayashi, and T. Iwayanagi, J. Vac. Sci. Technol. B 9, 278 (1991).
- H. Watanabe, H. Sumitani, T. Kumada, M. Inoue, K. Marumoto, and Y. Matsui, *Jpn. J. Appl. Phys.* 34, 6780 (1995).
- 22. M. Zuniga, G. Wallraff, and A. R. Neureuther, *Proc. SPIE* **2438**, 113 (1995).

- J. Nakamura, H. Ban, K. Deguchi, and A. Tanaka, *Jpn. J. Appl. Phys.* 30, 2619 (1991).
- 24. J. W. Thackeray, T. Adams, M. F. Cronin, M. Denison, T. H. Fedynyshyn, J. Georger, J. M. Mori, G. W. Orsula, and R. Sinta, J. Photopolymer Sci. Technol. 3, 619 (1994).
- T. Itani, H. Yoshino, S. Hashimoto, M. Yamana, N. Samoto, and K. Kasama, J. Vac. Sci. Technol. B 14, 4226 (1996).
- T. Itani, H. Yoshino, S. Hashimoto, M. Yamana, N. Samoto, and K. Kasama, J. Vac. Sci. Technol. B 15, 2541 (1997).
- T. Itani, H. Yoshino, S. Hashimoto, M. Yamana,
  N. Samoto, and K. Kasama, *Jpn. J. Appl. Phys.* 35, Pt. 1,
  No. 12B, 6501 (1996).
- A. A. Krasnaperova, M. Khan, S. Rhyner, J. W. Taylor, Y. Zhu, and F. Cerrina, J. Vac. Sci. Technol. B 12, 3900 (1994).
- C. Coenjarts, J. Cameron, N. Deschamps, D. Hambly, G. Pohlers, J. C. Scaiano, R. Sinta, S. Virdee, and A. Zampini, *Proc. SPIE* 3678, 1062 (1999).
- S. V. Postnikov, M. D. Stewart, H. V. Tran, M. Nierode, D. R. Madieros, T. Cao, J. Beyers, S. E. Webber, and C. G. Willson, J. Vac. Sci. Technol. B 17, 3335 (1999); E. Croffie, M. Cheng, and A. Neureuther, J. Vac. Sci. Technol. B 17, 3339 (1999).
- 31. J. S. Petersen, C. A. Mack, J. Sturtevant, J. D. Byers, and D. A. Miller, *Proc. SPIE* **2438**, 167 (1995).
- 32. A. Zuniga and A. R. Neureuther, J. Vac. Sci. Technol. B 14, 4221 (1996).
- G. Wallraff, W. Hinsberg, F. Houle, M. Morrison, C. Larson, M. Sanchez, J. Hoffnagle, P. Brock, and G. Breyta, SPIE Advances in Resist Technology and Processing XVI 3678, 138 (1999).
- 34. W. Hinsberg and F. Houle, U.S. Patents 5,446,870 (1995) and 5,826,065 (1998).
- T. DeV. Naylor, in Comprehensive Polymer Science,
  G. Allen and J. Bevington, Eds., Pergamon Press,
  New York, 1989, Ch. 20.
- Y. Kawai, A. Otaka, A. Tanaka, and T. Matsuda, *Jpn. J. Appl. Phys.* 33, 7023 (1994).
- 37. K. Asakawa, T. Oshirogouchi, and M. Nakase, SPIE Advances in Resist Technology and Processing XII 2438, 563 (1995)
- 38. W. Huang, SPIE Advances in Resist Technology and Processing XVI 3678, 1040 (1999).
- S. Funato, N. Kawasaki, Y. Kinoshita, S. Masuda, H. Okazaki, M. Padmanaban, T. Yamamoto, and G. Pawlowski, SPIE Advances in Resist Technology and Processing XIII 2724, 186 (1996).
- W. Hinsberg, F. Houle, M. Sanchez, M. Morrison,
  G. Wallraff, C. Larson, J. Hoffnagle, P. Brock, and
  G. Breyta, SPIE Advances in Resist Technology and Processing XVII 3999, 148 (2000).
- 41. J. Guillet, *Polymer Photophysics and Photochemistry*, Cambridge University Press, New York, 1985, Ch. 3.

Received September 21, 2000; accepted for publication January 11, 2001

William D. Hinsberg IBM Research Division, Almaden Research Center, 650 Harry Road, San Jose, California 95120 (hnsbrg@almaden.ibm.com). Dr. Hinsberg is a Research Staff Member in the Science and Technology Department at the IBM Almaden Research Center. He received a B.S. degree in chemistry from the University of Michigan at Ann Arbor, and a Ph.D. degree in chemistry from the California Institute of Technology (1980). In 1982, following a postdoctoral position at Stanford University, he joined the IBM General Products Division, where he worked on thin-film process chemistry for magnetic recording devices. He joined the IBM Research Division in 1983 to study the chemistry of new photoresist materials. Currently, Dr. Hinsberg is carrying out fundamental studies of materials for nanolithographic applications. He has received the AIChE NorCal Section Chemical Engineering Excellence Award for Research Project of the Year (1999), the Leo J. Friend Award of the American Chemical Society for his paper on DNA chips (1998), an IBM Corporate Environmental Affairs Excellence Award (1998) for simulator development, an IBM Supplemental Patent Award (1996), IBM Outstanding Technical Achievement Awards for deep-UV resist technology (1999) and solvent replacement in photoresist (1994), IBM Outstanding Technical Achievement and Outstanding Contribution Awards for thick-film resist technology, and an IBM Computational Chemistry Prize (1990). Dr. Hinsberg was named a Top Inventor of IBM in 1992. He is a coauthor of 70 publications and 23 U.S. and foreign patents.

Frances A. Houle IBM Research Division, Almaden Research Center, 650 Harry Road, San Jose, California 95120 (houle@almaden.ibm.com). Dr. Houle is a Research Staff Member in the Science and Technology Department at the IBM Almaden Research Center. She received a B.A. degree cum laude from the University of California at Irvine (1974) and a Ph.D. degree from the California Institute of Technology (1979), both in chemistry. She joined the IBM Research Division in 1980 after an appointment as an IBM Postdoctoral Fellow at the University of California at Berkeley. Dr. Houle's current research is in fundamental studies of deep-UV photoresist chemistry and fabrication of sub-100-nm structures, and development of stochastic modeling methods for simulation of complex chemical reactions and transport. She has received the 1999 AIChE NorCal Section Award for Chemical Engineering Excellence for Research Project of the Year, an IBM Corporate Environmental Affairs Excellence

Award (1998), an IBM Computational Chemistry Prize (1990), an IBM Outstanding Innovation Award for laser deposition of metals (1990), and an IBM Supplemental Patent Award (1996) for her work on surface processing and simulation algorithms. Dr. Houle is a coauthor of more than 75 papers and 16 U.S. and foreign patents. She is a Fellow of the American Vacuum Society, a Fellow of the American Physical Society, and a member of the American Chemical Society, the Materials Research Society, and the American Association for the Advancement of Science.

Martha I. Sanchez IBM Research Division, Almaden Research Center, 650 Harry Road, San Jose, California 95120 (msanchez@almaden.ibm.com). Ms. Sanchez is a Staff Engineer in the Science and Technology Department at the IBM Almaden Research Center. She received her B.S. and M.S. degrees in chemical engineering from the University of Maryland at College Park and Stanford University, respectively, and joined IBM in 1982. Her interests are in polymer processing and material characterization of polymers using techniques such as optical microscopy, scanning electron microscopy, atomic force microscopy, and infrared spectroscopy. She is a coauthor of approximately 30 publications and three patents, and is a member of the Society of Photo-Optical Instrumentation Engineers. In 1992, she received the Arthur K. Doolittle Award from the American Chemical Society.

Gregory M. Wallraff IBM Research Division, Almaden Research Center, 650 Harry Road, San Jose, California 95120 (gmwall@almaden.ibm.com). Dr. Wallraff is a Research Staff Member in the Science and Technology Department at the IBM Almaden Research Center. He received a Ph.D. degree in chemistry from the University of Utah, and has been a Research Staff Member since 1987. His research interests include mechanistic organic chemistry, studies of the chemistry and physics of polymeric thin films, design of lithographic resist systems, novel applications of lithography including DNA chips, and design of materials for 157-nm lithography. Dr. Wallraff received the 1998 Leo J. Friend Award of the American Chemical Society for his paper on DNA chips; he is a coauthor of more than 30 publications and 15 patents.